*Journal of Naval Architecture and Marine Engineering*
*June, 2021*
http://dx.doi.org/10.3329/jname.v18i1.33024 *http://www.banglajol.info*

# DIFFUSION-THERMO AND HEAT SOURCE EFFECTS ON THE UNSTEADY RADIATIVE MHD BOUNDARY LAYER SLIP FLOW PAST AN INFINITE VERTICAL POROUS PLATE

**M. Venkateswarlu[1*] and D. V. Lakshmi[2]**

[1]Department of Mathematics, V. R. Siddhartha Engineering College, Vijayawada, Krishna (Dist), A. P, India, PIN : 520 007.
Email*: mvsr2010@gmail.com
[2]Department of Mathematics, Bapatla Engineering College, Bapatla, Guntur (Dist), A. P, India, PIN : 522 102.
Email: himaja96@gmail.com

**Abstract:**

*The heat and mass transfer characteristics of the nonlinear, unsteady, radiative MHD boundary layer slip flow of a chemically reacting fluid past an infinite vertical porous plate are taken into account in this study. The effect of physical parameters are accounted for two distinct types of thermal boundary conditions namely prescribed uniform wall temperature thermal boundary condition and prescribed heat flux thermal boundary condition. Exact solution of the governing equations for the fluid velocity, temperature, and concentration are obtained by using two term perturbation technique subject to physically appropriate boundary conditions. The expressions of skin friction, Nusselt number, and Sherwood number are also derived. The numerical values of fluid velocity, temperature, and concentration are displayed graphically whereas those of shear stress, rate of heat transfer, and rate of mass transfer at the plate are presented in tabular form for various values of pertinent flow parameters. In particular, slip parameter accelerates the fluid velocity whereas it has a reverse effect on the skin friction coefficient for both PST and PHF boundary conditions. This study is a cutting-edge simulation tool to maximize efficiency in design and operation in Naval Architecture, Offshore and Marine Engineering, as well as in the Renewable Energy sector. Results are compared with the literature in the limiting case.*

***Keywords:*** MHD, Dufour effect, porous medium, heat source, radiation of absorption, slip condition.

## NOMENCLATURE

| | |
|---|---|
| $a^*$ | mean absorption coefficient |
| $A$ | A real positive constant |
| $B_o$ | uniform magnetic field ( *Tesla* ) |
| $C$ | species concentration ( *moles / litre* ) |
| $C_f$ | skin-friction coefficient |
| $C_\infty$ | uniform concentration ( *moles / litre* ) |
| $C_w$ | species concentration at the wall |
| $c_p$ | specific heat at constant pressure |
| $c_s$ | concentration susceptibility |
| $D_m$ | mass diffusivity coefficient ( $m^2\ s^{-1}$ ) |
| $Du$ | Dufour number |
| $Gm$ | solutal Grashof number |
| $Gr$ | thermal Grashof number |
| $g$ | acceleration due to gravity ( $m\,s^{-2}$ ) |
| $h$ | non-dimensional slip parameter |
| $H$ | non- dimensional heat source parameter |
| $Sc$ | Schmidt number |
| $j_w$ | mass flux |
| $K_1$ | permeability of porous medium |
| $K$ | non-dimensional permeability |
| $K_r^*$ | dimensional chemical reaction |
| $Kr$ | non-dimensional chemical reaction |
| $k_T$ | thermal conductivity of the fluid |
| $M$ | magnetic parameter |
| $N$ | radiation parameter |
| $Nu$ | Nusselt number |
| $n$ | frequency of oscillation |
| $p$ | fluid pressure ( $Pa$ ) |
| Pr | Prandtl number |
| $Q$ | non dimensional radiation of absorption |
| $Q_o$ | dimensional heat source parameter |
| $Q_1$ | dimensional radiation of absorption |
| $q_r$ | radiating flux vector |
| $q_w$ | heat flux |
| $\omega$ | A scaled frequency |

 Received on: July, 2017

| | | | |
|---|---|---|---|
| $Sh$ | Sherwood number | $\phi$ | A scaled concentration ( *moles / litre* ) |
| $T$ | fluid temperature ( $K$ ) | $\alpha$ | thermal conductivity ( $m^2\ s^{-1}$ ) |
| $T_\infty$ | uniform temperature ( $K$ ) | $\rho$ | fluid density ( $kg\ m^{-3}$ ) |
| $T_w$ | fluid temperature at wall ( $K$ ) | $\sigma_e$ | electrical conductivity ( $V\ m^{-1}$ ) |
| $t$ | dimensional time ( $s$ ) | $\tau$ | non dimensional time ( $s$ ) |
| $u$ | fluid velocity in $x-$direction ( $m\,s^{-1}$ ) | $\tau_w$ | shear stress |
| $U_o$ | characteristic velocity ( $m\,s^{-1}$ ) | $\psi$ | A scaled velocity ( $m\,s^{-1}$ ) |
| $U_\infty$ | dimensional free stream | $\psi_\infty$ | non dimensional free stream |
| $v$ | fluid velocity in $y-$ direction ( $m\,s^{-1}$ ) | $\eta$ | A scaled coordinate ( $m$ ) |
| $V_o$ | scale of suction velocity ( $m\,s^{-1}$ ) | $\theta$ | A scaled temperature ( $K$ ) |
| ***Greek symbols*** | | $\sigma^*$ | Stefan-Boltzmann constant |
| $\beta_c$ | coefficient of species concentration | $\varepsilon$ | A small positive constant |
| $\beta_T$ | coefficient of thermal expansion | $\gamma$ | dimensional slip parameter ( $m$ ) |

## 1. Introduction

The convection problem in porous media has important applications in geothermal reservoirs, geothermal energy extractions, coal gasification, iron blast furnaces, ground water hydrology, wall cooled catalytic reactors, energy efficient drying processes, solar power collectors, cooling of nuclear fuel in shipping flasks, cooling of electronic equipments and natural convection in earth's crust. Convection in porous media was documented by Nield and Bejan (1999). Subsequently, physical articles on porous media can be found in Adesanya and Makinde (2014); Manjula et al. (2015); Venkateswarlu and Padma (2015); Venkateswarlu and Lakshmi (2016); Rajakumar et al. (2018a, 2018b & 2020a); and Venkateswarlu et al. (2019b). Sharma and Saboo (2017) analyzed the heat and mass transfer with viscous dissipation in horizontal channel partially occupied by porous medium in the presence of oscillatory suction. Venkateswarlu et al. (2018) considered the influence of Hall current and heat source on MHD flow of a rotating fluid in a parallel porous plate channel. Raju et al. (2018) studied the ramped temperature influence on MHD convective chemically reactive and absorbing fluid past an exponentially accelerated vertical porous plate. Venkateswarlu et al. (2019a) reported the Soret and Dufour effects on radiative hydromagnetic flow of a chemically reacting fluid over an exponentially accelerated inclined porous plate in presence of heat absorption and viscous dissipation. Baitharu et al. (2020) considered the heat and mass transfer effect on a radiative second grade MHD flow in a porous medium over a stretching sheet. Rajakumar et al. (2020b) presented the unsteady MHD Casson dissipative fluid flow past a semi-infinite vertical porous plate with radiation absorption and chemical reaction in presence of heat generation.

The study of MHD flows have stimulated considerable interest due to its important physical applications in solar physics, meteorology, power generating systems, aeronautics and missile aerodynamics, cosmic fluid dynamics and in the motion of Earth's core [Sparrow and Cess (1961), Cramer & Pai (1973)]. In a broader sense, MHD has applications in three different subject areas, such as astrophysical, geophysical and engineering problems. Other remarkable research works are due to Rout et al. (2016); Seth et al. (2017); Malapati and Dasari (2017); Thirupathi and Mishra (2018); Venkateswarlu and Makinde (2018); Tirupathi and Satya Narayana (2020); and Tirupathi and Magagula (2020). Venkateswarlu et al. (2019d) presented the influence of heat generation and viscous dissipation on hydromagnetic fully developed natural convection flow in a vertical micro-channel. Rajput and Kumar (2019) analyzed the effects of radiation and chemical reaction on MHD flow past a vertical plate with variable temperature and mass diffusion. Rout et al. (2019) reported the effect of viscous dissipation on Cu-water and Cu-kerosene nanofluids of axisymmetric radiative squeezing flow. Venkateswarlu and Bhaskar (2020) presented the entropy generation and Bejan number analysis of MHD Casson fluid flow in a micro-channel with Navier slip and convective boundary conditions. Shankar Goud et al. (2020) presented the thermal radiation and Joule heating effects on a magnetohydrodynamic Casson nanofluid flow in the presence of chemical reaction through a non-linear inclined porous stretching sheet.

The Dufour and Soret effects in the combined heat and mass transfer processes, due to the thermal diffusion flux resulting from the temperature gradients and the thermal energy flux resulting from concentration gradients may be significant in the areas of chemical engineering and geosciences. The hydromagnetic mixed convection flow with Soret and Dufour effects past a vertical plate embedded in a porous medium was investigated by Makinde

(2011). Seini and Makinde (2013) presented numerical solutions for hydromagnetic flow with Dufour and Soret effects past a vertical plate embedded in porous media. Venkateswarlu and Kumar (2017) reported the Soret and heat source effects on MHD flow of a viscous fluid in a parallel porous plate channel in presence of slip condition. Vedavathi et al. (2015) examined the radiation and mass transfer effects on unsteady MHD convective flow past an infinite vertical plate with Dufour and Soret effects. Venkateswarlu et al. (2019c) presented the influence of Hall current and thermal diffusion on radiative hydromagnetic flow of a rotating fluid in presence of heat absorption. Other related considered literatures can be found in Venkateswarlu and Lakshmi (2017); Venkateswarlu et al. (2020); Thirupathi et al. (2020); and Balamurugan et al. (2021).

The objective of the present study is to investigate the Diffusion-thermo and heat source effects on the unsteady radiative MHD boundary layer slip flow of a chemically reacting fluid past an infinite vertical porous plate. Therefore, in the present work, the physical problem as described in Pal and Talukdar (2010) is considered. We should in prior emphasize that our intention is not to reproduce the results of Pal and Talukdar (2010). In fact, the model that we consider differs considerably from that of Pal and Talukdar (2010) in that we use a better approach in the formulation, introduce a Dufour effect and make use of two kinds of thermal boundary conditions, namely, prescribed wall temperature (PST) and prescribed heat flux (PHF). Analytical closed form solutions are presented for the momentum, the concentration, and the energy equations using some proper change of variables. By means of the presented solutions, the flow field, the thermal, and hydrodynamics response of the system such as the skin friction, concentration transfer and heat transfer coefficients of physical importance can be rigorously investigated.

The following strategy is pursued in the rest of the paper. Section two presents the formation of the problem. The analytical solutions are presented in section three. Section four contains the validation of numerical code. Results are discussed in section five and finally section six provides a conclusion of the paper.

## 2. Formation of the Problem

Consider an unsteady, nonlinear, radiative MHD free convection and mass transfer flow of an incompressible, viscous and electricity conducting fluid past an infinite vertical porous plate in the presence of a uniform transverse magnetic field of strength $B_o$ . In view of the assumptions made by Pal and Talukdar (2010), as well as of the usual Boussinesq's approximation, the governing equations can be written as:

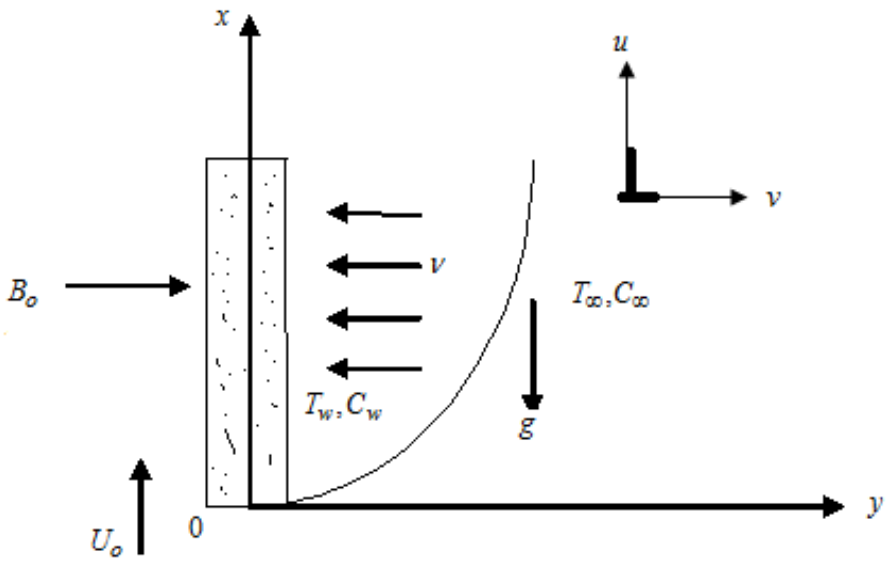


Fig.1: Geometry of the problem.

Continuity equation:

$$\frac{\partial v}{\partial y} = 0 \tag{1}$$

Momentum equation:

$$\frac{\partial u}{\partial t}+v\frac{\partial u}{\partial y}=-\frac{1}{\rho}\frac{dp}{dx}+\nu\frac{\partial^2 u}{\partial y^2}-\left[\frac{\sigma_e B_0^2}{\rho}+\frac{\nu}{K_1}\right]u+g\beta_T\left(T-T_\infty\right)+g\beta_c\left(C-C_\infty\right) \tag{2}$$

Energy equation:

$$\frac{\partial T}{\partial t}+v\frac{\partial T}{\partial y}=\alpha\frac{\partial^2 T}{\partial y^2}-\frac{Q_o}{\rho c_p}\left(T-T_\infty\right)-\frac{1}{\rho c_p}\frac{\partial q_r}{\partial y}+\frac{Q_1}{\rho c_p}\left(C-C_\infty\right)+\frac{D_m k_T}{c_s c_p}\frac{\partial^2 C}{\partial y^2} \tag{3}$$

Diffusion equation;

$$\frac{\partial C}{\partial t}+v\frac{\partial C}{\partial y}=D_m\frac{\partial^2 C}{\partial y^2}-K_r^*\left(C-C_\infty\right) \tag{4}$$

The initial and boundary conditions are given as follows

$$\left.\begin{aligned}&u=\gamma\frac{du}{dy},\quad T=T_w+\varepsilon\left(T_w-T_\infty\right)\mathrm{e}^{nt}\ \left(\text{for PST}\right),\ \alpha\frac{\partial T}{\partial y}=-q_w\left(1+\varepsilon e^{nt}\right)\left(\text{for PHF}\right),\\&C=C_w+\varepsilon\left(C_w-C_\infty\right)\mathrm{e}^{nt}\quad\text{at}\quad y=0\\&u\to U_\infty=U_o\left(1+\varepsilon e^{nt}\right),\ T\to T_\infty,\quad C\to C_\infty\ \text{as}\ y\to\infty\end{aligned}\right\} \tag{5}$$

Following Rapits (2011), we adopt the Rosseland approximation for the radiative flux vector $q_r$, namely

$$\frac{\partial q_r}{\partial y}=-4a^*\sigma^*\left(T_\infty^4-T^4\right) \tag{6}$$

We assume that the difference between fluid temperature $T$ and free stream temperature $T_\infty$ within the flow is sufficiently small such that $T^4$ may be expressed as a linear function of the temperature. This is accomplished by expanding in Taylor series $T^4$ about the free stream temperature $T_\infty$ and neglecting the second and higher order terms, we have

$$T^4\cong 4T_\infty^3T-3T_\infty^4 \tag{7}$$

Using Eqs. (6) and (7) in Eq. (3) we obtain

$$\frac{\partial T}{\partial t}+v\frac{\partial T}{\partial y}=\alpha\frac{\partial^2 T}{\partial y^2}-\frac{Q_o}{\rho c_p}\left(T-T_\infty\right)+\frac{Q_1}{\rho c_p}\left(C-C_\infty\right)+\frac{D_m k_T}{c_s c_p}\frac{\partial^2 C}{\partial y^2}-\frac{16a^*\sigma^*T_\infty^3}{\rho c_p}\left(T-T_\infty\right) \tag{8}$$

It is clear from Eq. (1) that the suction velocity at the plate is a function of time only. Assuming that, the suction velocity takes the following exponential form:

$$v=-V_o\left(1+\varepsilon Ae^{nt}\right) \tag{9}$$

Here the negative sign indicates that the suction is towards the plate.
Outside the boundary layer, Equation (2) gives [see, Kim (2000)]

$$-\frac{1}{\rho}\frac{\partial p}{\partial x}=\frac{dU_\infty}{dt}+\frac{\sigma_e B_o^2}{\rho}U_\infty+\frac{\nu}{K_1}U_\infty \tag{10}$$

By introducing the non-dimensional variables as follows

$$\psi=\frac{u}{U_o},\eta=\frac{V_o}{\nu}y,\psi_\infty=\frac{U_\infty}{U_o},\omega=\frac{\nu}{V_o^2}n,\tau=\frac{V_o^2}{\nu}t,h=\frac{V_o}{\nu}\gamma,\theta=\frac{T-T_\infty}{T_w-T_\infty},\phi=\frac{C-C_\infty}{C_w-C_\infty} \tag{11}$$

Eqs. (2), (4) and (8) reduce to the following non-dimensional form

$$\frac{\partial\psi}{\partial\tau}-\left(1+\varepsilon Ae^{\omega\tau}\right)\frac{\partial\psi}{\partial\eta}=\frac{d\psi_\infty}{d\tau}+\frac{\partial^2\psi}{\partial\eta^2}+Gr\theta+Gm\phi+\left[M+\frac{1}{K}\right]\left(\psi_\infty-\psi\right) \tag{12}$$

$$\frac{\partial\theta}{\partial\tau}-\left(1+\varepsilon Ae^{\omega\tau}\right)\frac{\partial\theta}{\partial\eta}=\frac{1}{\mathrm{Pr}}\frac{\partial^2\theta}{\partial\eta^2}-\left(N+H\right)\theta+Du\frac{\partial^2\phi}{\partial\eta^2}+Q\phi \tag{13}$$

$$\frac{\partial\phi}{\partial\tau}-\left(1+\varepsilon Ae^{\omega\tau}\right)\frac{\partial\phi}{\partial\eta}=\frac{1}{Sc}\frac{\partial^2\phi}{\partial\eta^2}-Kr\phi \tag{14}$$

Here $Gr = \frac{g\beta_T (T_w - T_\infty)\nu}{U_o V_o^2}$, $Gm = \frac{g\beta_c (C_w - C_\infty)\nu}{U_o V_o^2}$, $M = \frac{\sigma_e B_o^2 \nu}{\rho V_o^2}$, $K = \frac{K_1 V_o^2}{\nu^2}$, $\Pr = \frac{\nu}{\alpha}$, $N = \frac{16a^*\sigma^*\nu T_\infty^3}{\rho c_p V_o^2}$, $H = \frac{Q_o \nu}{\rho c_p V_o^2}$, $Du = \frac{D_m (C_w - C_\infty) k_T}{c_s c_p (T_w - T_\infty)\nu}$, $Q = \frac{Q_1 (C_w - C_\infty)\nu}{\rho c_p (T_w - T_\infty) V_o^2}$, $Sc = \frac{\nu}{D_m}$, and $Kr = \frac{\nu}{V_o^2} K_r^*$.

The corresponding initial and boundary conditions can be written as

$$\left.\begin{aligned} &\psi = h\frac{\partial \psi}{\partial \eta},\ \theta = 1 + \varepsilon e^{\omega\tau}\ (\text{for PST}), \frac{\partial \theta}{\partial \tau} = -\left[1 + \varepsilon e^{\omega\tau}\right](\text{for PHF}),\ \phi = 1 + \varepsilon e^{\omega\tau}\ \text{ at }\ \eta = 0 \\ &\psi \to \psi_\infty = 1 + \varepsilon e^{\omega\tau},\quad \theta \to 0,\qquad \phi \to 0 \qquad \text{as} \quad \eta \to \infty \end{aligned}\right\} \tag{15}$$

Given the velocity, temperature, and concentration fields in the boundary layer, the shear stress $\tau_w$, the heat flux $q_w$, and mass flux $j_w$ are obtained by

$$\tau_w = \mu\left[\frac{\partial u}{\partial y}\right]_{y=0} \tag{16}$$

$$q_w = -\alpha\left[\frac{\partial T}{\partial y}\right]_{y=0} \tag{17}$$

$$j_w = -D_m\left[\frac{\partial C}{\partial y}\right]_{y=0} \tag{18}$$

In non-dimensional form the skin-friction coefficient $C_f$, heat transfer coefficient $Nu$, and mass transfer coefficient $Sh$ are defined as

$$C_f = \frac{\tau_w}{\rho U_o^2} \tag{19}$$

$$Nu = \frac{\nu q_w}{\alpha V_o (T_w - T_\infty)} \tag{20}$$

$$Sh = \frac{\nu j_w}{D_m V_o (C_w - C_\infty)} \tag{21}$$

Using the Eqs. (16) to (18) into Eqs. (19) to (21), we can obtain

$$C_f = \left[\frac{\partial \psi}{\partial \eta}\right]_{\eta=0} \tag{22}$$

$$Nu = -\left[\frac{\partial \theta}{\partial \eta}\right]_{\eta=0} \tag{23}$$

$$Sh = -\left[\frac{\partial \phi}{\partial \eta}\right]_{\eta=0} \tag{24}$$

## 3. Solution of the Problem

Eqs. (12) to (14) are coupled non-linear partial differential equations and these cannot be solved in closed form. So, we reduce these non-linear partial differential equations into a set of ordinary differential equations, which can be solved analytically. This can be done by assuming the trial solutions for the velocity, temperature and concentration of the fluid as [see, Siva Kumar et al. (2016), Venkateswarlu et al. (2016)]

$$\psi(\eta,\tau) = \psi_o(\eta) + \varepsilon\, \mathrm{e}^{\omega\tau}\, \psi_1(\eta) + o\left(\varepsilon^2\right) \tag{25}$$

$$\theta(\eta,\tau) = \theta_0(\eta) + \varepsilon\, \mathrm{e}^{\omega\tau}\, \theta_1(\eta) + o\left(\varepsilon^2\right) \tag{26}$$

$$\phi(\eta,\tau) = \phi_0(\eta) + \varepsilon\, \mathrm{e}^{\omega\tau}\, \phi_1(\eta) + o\left(\varepsilon^2\right) \tag{27}$$

Substituting Eqs. (25) to (27) into Eqs. (12) to (14), then we obtain the following ordinary differential equations

$$\psi_o'' + \psi_o' - \left[M + \frac{1}{K}\right]\psi_o = -\left[Gr\theta_o + Gm\phi_o + M + \frac{1}{K}\right] \tag{28}$$

$$\psi_1'' + \psi_1' - \left[M + \frac{1}{K} + \omega\right]\psi_1 = -\left[Gr\theta_1 + Gm\phi_1 + M + \frac{1}{K} + \omega + A\psi_o'\right] \tag{29}$$

$$\theta_o'' + \Pr\theta_o' - \Pr(N + H)\theta_o = -\Pr\left[Du\phi_o'' + Q\phi_o\right] \tag{30}$$

$$\theta_1'' + \Pr\theta_1' - \Pr(N + H + \omega)\theta_1 = -\Pr\left[Du\phi_1'' + Q\phi_1 + A\theta_o'\right] \tag{31}$$

$$\phi_o'' + Sc\phi_o' - ScKr\phi_o = 0 \tag{32}$$

$$\phi_1'' + Sc\phi_1' - Sc(Kr + \omega)\phi_1 = -ASc\phi_o' \tag{33}$$

where the prime denotes the ordinary differentiation with respect to $\eta$.

The corresponding initial and boundary conditions can be written as

$$\left.\begin{aligned} &\psi_o = h\psi_o',\ \psi_1 = h\psi_1',\ \theta_o = 1,\ \theta_1 = 1(\text{for PST}), \theta_o = -1,\ \theta_1 = -1(\text{for PHF}), \phi_o = 1,\ \phi_1 = 1 \quad \text{at} \quad \eta = 0 \\ &\psi_o = 1, \quad \psi_1 = 1, \quad \theta_o \to 0, \qquad \theta_1 \to 0, \quad \phi_o \to 0, \qquad \phi_1 \to 0 \quad \text{as} \quad \eta \to \infty \end{aligned}\right\} \tag{34}$$

The analytical solutions of Eqs. (28) to (33) in the case of PST with the boundary conditions in Eq. (34), are given by

$$\psi_o = 1 + A_{21}\,\mathrm{e}^{-m_1\eta} - A_{22}\,\mathrm{e}^{-m_3\eta} + A_{28}\,\mathrm{e}^{-m_5\eta} \tag{35}$$

$$\psi_1 = 1 + A_{39}\,\mathrm{e}^{-m_1\eta} + A_{40}\,\mathrm{e}^{-m_2\eta} - A_{41}\,\mathrm{e}^{-m_3\eta} - A_{42}\,\mathrm{e}^{-m_4\eta} + A_{43}\,\mathrm{e}^{-m_5\eta} + A_{49}\,\mathrm{e}^{-m_6\eta} \tag{36}$$

$$\theta_o = A_8\,\mathrm{e}^{-m_3\eta} - A_7\,\mathrm{e}^{-m_1\eta} \tag{37}$$

$$\theta_1 = A_{18}\,\mathrm{e}^{-m_4\eta} - A_{15}\,\mathrm{e}^{-m_1\eta} - A_{16}\,\mathrm{e}^{-m_2\eta} + A_{17}\,\mathrm{e}^{-m_3\eta} \tag{38}$$

$$\phi_o = \mathrm{e}^{-m_1\eta} \tag{39}$$

$$\phi_1 = A_3\,\mathrm{e}^{-m_1\eta} + A_4\,\mathrm{e}^{-m_2\eta} \tag{40}$$

By substituting Eqs. (35) to (40) into Eqs. (25) to (27), we obtained solutions for the fluid velocity, temperature, and concentration in the case of PST as follows

$$\psi(\eta,\tau) = \left[1 + A_{21}\,\mathrm{e}^{-m_1\eta} - A_{22}\,\mathrm{e}^{-m_3\eta} + A_{28}\,\mathrm{e}^{-m_5\eta}\right] + \varepsilon\,\mathrm{e}^{\omega\tau}\begin{bmatrix} 1 + A_{39}\,\mathrm{e}^{-m_1\eta} + A_{40}\,\mathrm{e}^{-m_2\eta} - A_{41}\,\mathrm{e}^{-m_3\eta} - \\ A_{42}\,\mathrm{e}^{-m_4\eta} + A_{43}\,\mathrm{e}^{-m_5\eta} + A_{49}\,\mathrm{e}^{-m_6\eta} \end{bmatrix} \tag{41}$$

$$\theta(\eta,\tau) = \left[A_8\,\mathrm{e}^{-m_3\eta} - A_7\,\mathrm{e}^{-m_1\eta}\right] + \varepsilon\,\mathrm{e}^{\omega\tau}\left[A_{18}\,\mathrm{e}^{-m_4\eta} - A_{15}\,\mathrm{e}^{-m_1\eta} - A_{16}\,\mathrm{e}^{-m_2\eta} + A_{17}\,\mathrm{e}^{-m_3\eta}\right] \tag{42}$$

$$\phi(\eta,\tau) = \mathrm{e}^{-m_1\eta} + \varepsilon\,\mathrm{e}^{\omega\tau}\left[A_3\,\mathrm{e}^{-m_1\eta} + A_4\,\mathrm{e}^{-m_2\eta}\right] \tag{43}$$

Keeping in view, the assumptions made earlier, solutions to the fluid velocity and temperature profiles in the case of PHF are obtained and presented in the following form

$$\psi(\eta,\tau) = \left[1 + A_{21}\,\mathrm{e}^{-m_1\eta} - B_5\,\mathrm{e}^{-m_3\eta} + B_7\,\mathrm{e}^{-m_5\eta}\right] + \varepsilon\,\mathrm{e}^{\omega\tau}\begin{bmatrix} 1 + A_{39}\,\mathrm{e}^{-m_1\eta} + A_{40}\,\mathrm{e}^{-m_2\eta} - B_{11}\,\mathrm{e}^{-m_3\eta} - \\ B_{12}\,\mathrm{e}^{-m_4\eta} + B_{13}\,\mathrm{e}^{-m_5\eta} + B_{15}\,\mathrm{e}^{-m_6\eta} \end{bmatrix} \tag{44}$$

$$\theta(\eta,\tau) = \left[B_1\,\mathrm{e}^{-m_3\eta} - A_7\,\mathrm{e}^{-m_1\eta}\right] + \varepsilon\,\mathrm{e}^{\omega\tau}\left[B_4\,\mathrm{e}^{-m_4\eta} - A_{15}\,\mathrm{e}^{-m_1\eta} - A_{16}\,\mathrm{e}^{-m_2\eta} + B_3\,\mathrm{e}^{-m_3\eta}\right] \tag{45}$$

3.1. Skin friction: From the velocity field, the skin friction at the plate can be obtained as

$$C_{f\,\text{PST}} = \left[A_{22}m_3 - A_{21}m_1 - A_{28}m_5\right] + \varepsilon\,\mathrm{e}^{\omega\tau}\left[A_{41}m_3 + A_{42}m_4 - A_{39}m_1 - A_{40}m_2 - A_{43}m_5 - A_{49}m_6\right] \tag{46}$$

$$C_{f\,\text{PHF}} = \left[B_5m_3 - A_{21}m_1 - B_7m_5\right] + \varepsilon\,\mathrm{e}^{\omega\tau}\left[B_{11}m_3 + B_{12}m_4 - A_{39}m_1 - A_{40}m_2 - B_{13}m_5 - B_{15}m_6\right] \tag{47}$$

3.2. Nusselt number: From the temperature field, the heat transfer coefficient can be obtained as

$$Nu_{\text{PST}} = \left[A_8m_3 - A_7m_1\right] + \varepsilon e^{\omega\tau}\left[A_{17}m_3 + A_{18}m_4 - A_{15}m_1 - A_{16}m_2\right] \tag{48}$$

$$Nu_{\text{PHF}} = \left[B_1m_3 - A_7m_1\right] + \varepsilon e^{\omega\tau}\left[B_3m_3 + B_4m_4 - A_{15}m_1 - A_{16}m_2\right] \tag{49}$$

3. 3. Sherwood number: From the concentration field, the mass transfer coefficient can be obtained as

$$Sh = m_1 + \varepsilon e^{\omega\tau}\left[A_3m_1 + A_4m_2\right] \tag{50}$$

## 4. Validation of the Solution

Since Pal and Talukdar (2010) obtained the exact solution of fluid velocity considering prescribed wall temperature whereas we have obtained the solution for fluid velocity for the case of prescribed wall temperature and prescribed heat flux. To compare our results of skin friction with those [see, Tables 2, 3 and 4] of Pal and Talukdar (2010) as a special case in the absence of Dufour effect along with porous medium, we have computed the numerical values of skin friction for our problem as well as those of Pal and Talukdar (2010) which are presented in Table 1. It is revealed from Table 1 that, there is an excellent agreement between both the results.

Table 1: Validation with literature for $Du = 0$ and $K = \infty$.

| $h$ | $N$ | $Kr$ | Skin friction coefficient $C_f$ | | % error |
|---|---|---|---|---|---|
| | | | Pal and Talukdar (2010) | Present | |
| 0.0 | 2.0 | 0.10 | 6.4047 | 6.4048 | 0.0015 |
| 0.1 | 2.0 | 0.10 | 5.3082 | 5.3082 | 0.0000 |
| 0.3 | 2.0 | 0.10 | 3.9540 | 3.9541 | 0.0025 |
| 0.5 | 2.0 | 0.10 | 3.1503 | 3.1503 | 0.0000 |
| 0.3 | 1.0 | 0.10 | 4.1838 | 4.1838 | 0.0000 |
| 0.3 | 2.0 | 0.10 | 3.9540 | 3.9541 | 0.0025 |
| 0.3 | 3.0 | 0.10 | 3.8015 | 3.8016 | 0.0026 |
| 0.3 | 4.0 | 0.10 | 3.6901 | 3.6901 | 0.0000 |
| 0.3 | 2.0 | 0.00 | 4.0441 | 4.0442 | 0.0024 |
| 0.3 | 2.0 | 0.50 | 3.7512 | 3.7513 | 0.0026 |
| 0.3 | 2.0 | 0.75 | 3.6744 | 3.6744 | 0.0000 |
| 0.3 | 2.0 | 1.00 | 3.6149 | 3.6149 | 0.0000 |

## 5. Results and Discussion

In order to investigate the influence of various physical parameters such as thermal Grashof number $Gr$, solutal Grashof number $Gm$, magnetic parameter $M$, Permeability parameter $K$, Dufour number $Du$, Prandtl number $\Pr$, radiation parameter $N$, heat source parameter $H$, radiation of absorption parameter $Q$, mass diffusion parameter $Sc$, chemical reaction parameter $Kr$, slip parameter $h$, and time $\tau$ on the flow-field, fluid velocity $\psi$, temperature $\theta$, and concentration $\phi$ have been studied analytically and computed results of the analytical solutions are displayed graphically from Figs. 2 to 25. The numerical values of the skin friction coefficient, heat transfer coefficient, and mass transfer coefficient are presented in tabular form in tables 2 to 7. Matlab (2015a) program is written to generate numerical results of the present work. For the purposes of our numerical computations, we adopted the following parameter values: $Gr = 4$, $Gm = 2$, $M = 2$, $K = 5$, $\Pr = 0.71$, $N = 2$, $H = 1$, $Q = 2$, $Du = 5$, $Sc = 0.60$, $Kr = 1$, $\tau = 1$, $A = 0.5$, $\omega = 1$, $h = 0.2$, and $\varepsilon = 0.01$.

It is observed that from Figs. 2 to 25, fluid velocity $\psi$, temperature $\theta$, and concentration $\phi$ attain a distinctive maximum value near the surface of the plate and then decrease properly on increasing boundary layer coordinate $\eta$ to approach free stream value in both PST and PHF boundary conditions. The effects of thermal Grashof number and solutal Grashof number on the fluid velocity are presented in Figs. 2 and 3. Physically, thermal Grashof number signifies the relative strength of thermal buoyancy force to viscous hydrodynamic force in the boundary layer. Solutal Grashof number signifies the relative strength of species buoyancy force to viscous hydrodynamic force in the boundary layer. It is noticed that, thermal Grashof number and solutal Grashof number accelerates the fluid velocity for both PST and PHF boundary conditions. In Fig. 4 it is observed that, the fluid velocity decreases with an increase in the Magnetic parameter due to a rise in magnetic field intensity. The transversely imposed magnetic field on the conducting dusty fluid produced a Lorentz force which acts as a resistance to the flow, consequently, the velocity decreases for both PST and PHF boundary conditions. Fig. 5 also shows an increase in the dusty fluid velocity profiles with an increase in permeability parameter for both PST and PHF boundary conditions.

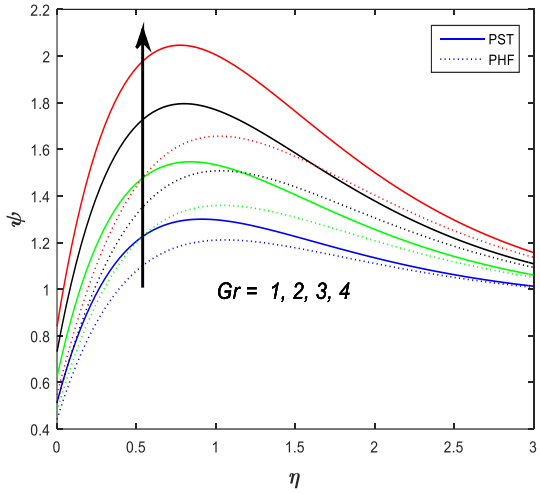


Fig. 2: Influence of $Gr$ on velocity profiles

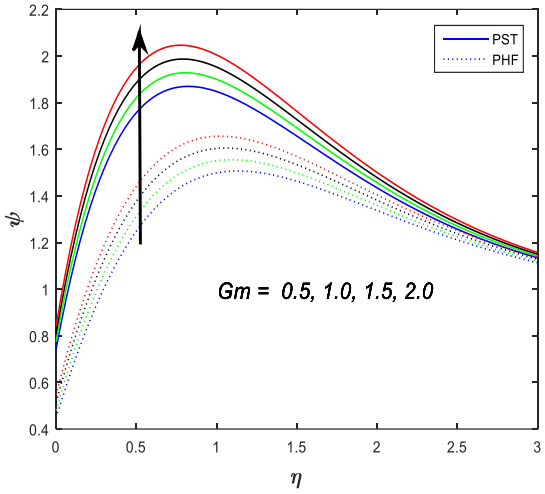


Fig. 3: Influence of $Gm$ on velocity profiles

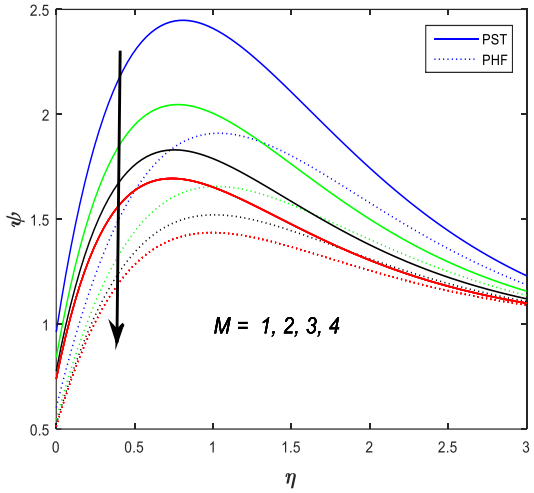


Fig. 4: Influence of $M$ on velocity profiles

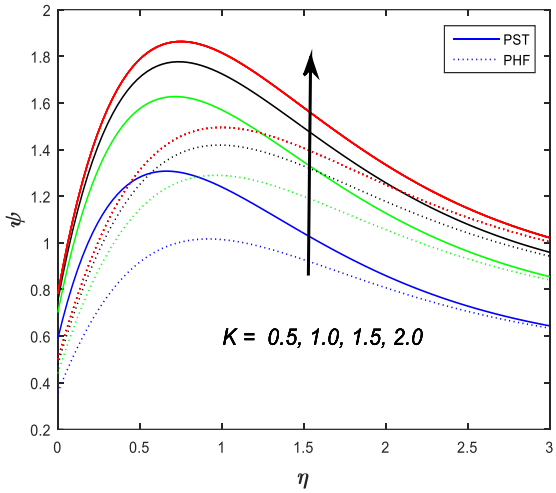


Fig. 5: Influence of $K$ on velocity profiles

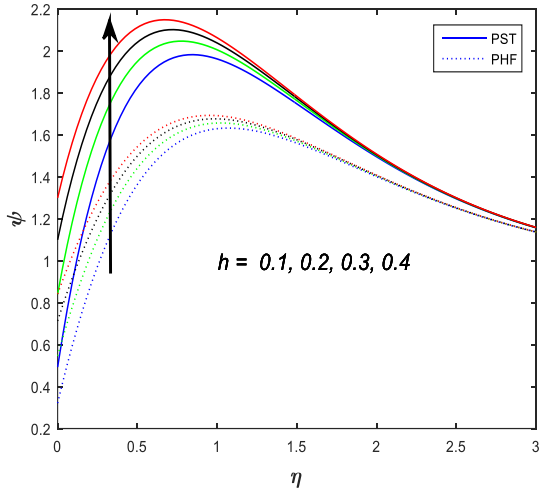


Fig. 6: Influence of $h$ on velocity profiles

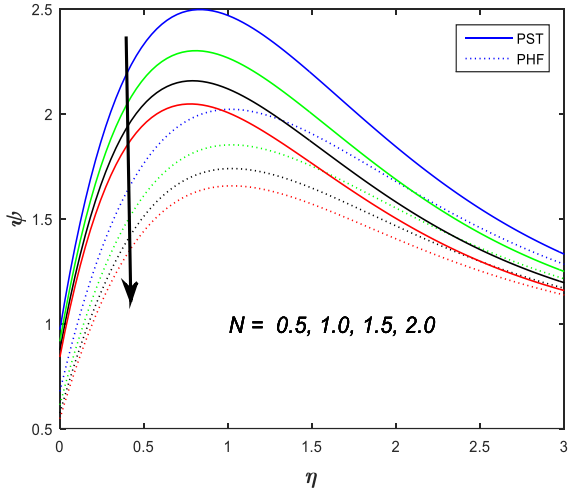


Fig. 7: Influence of $N$ on velocity profiles

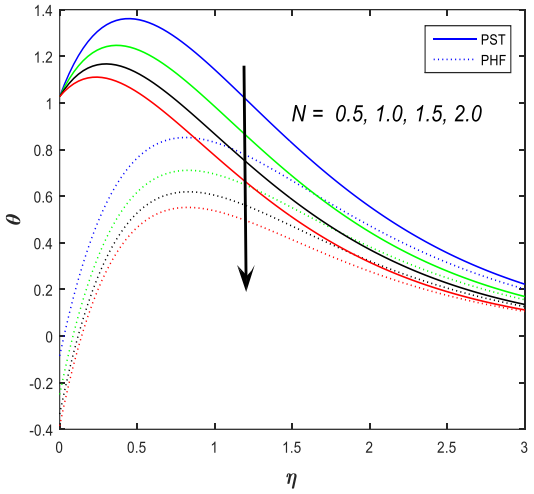


Fig. 8: Influence of $N$ on temperature profiles

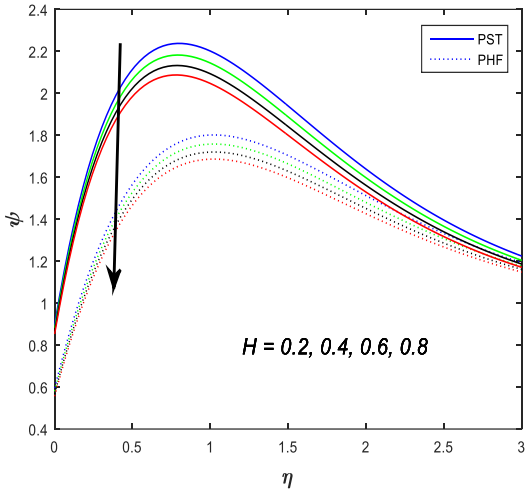


Fig. 9: Influence of $H$ on velocity profiles

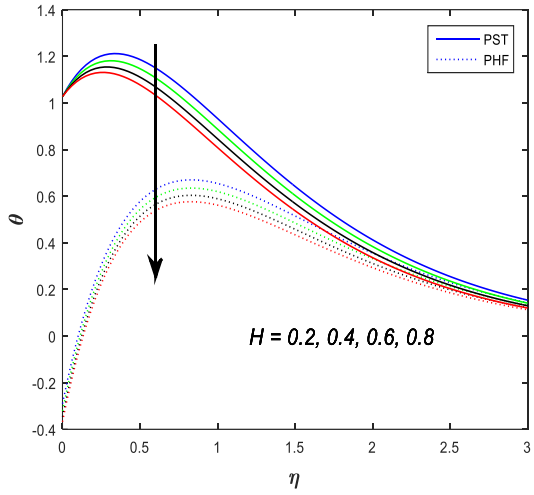


Fig. 10: Influence of $H$ on temperature profiles

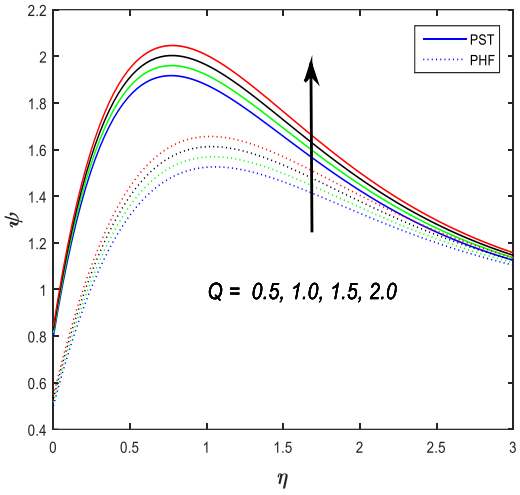


Fig. 11: Influence of $Q$ on velocity profiles

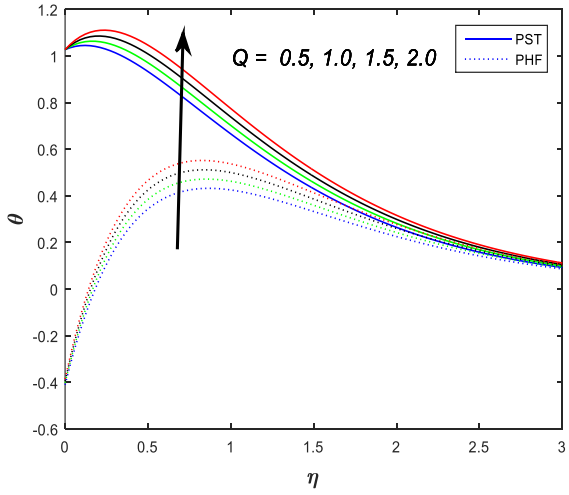


Fig. 12: Influence of $Q$ on temperature profiles

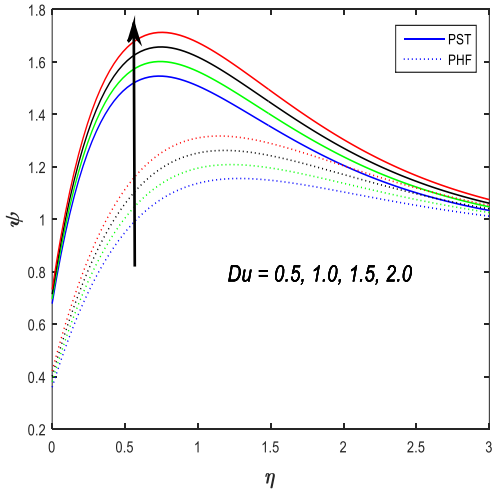


Fig. 13: Influence of $Du$ on velocity profiles

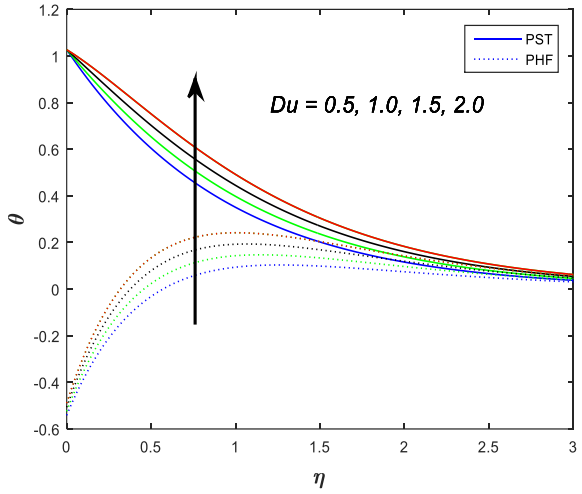


Fig. 14: Influence of *Du* on temperature profiles

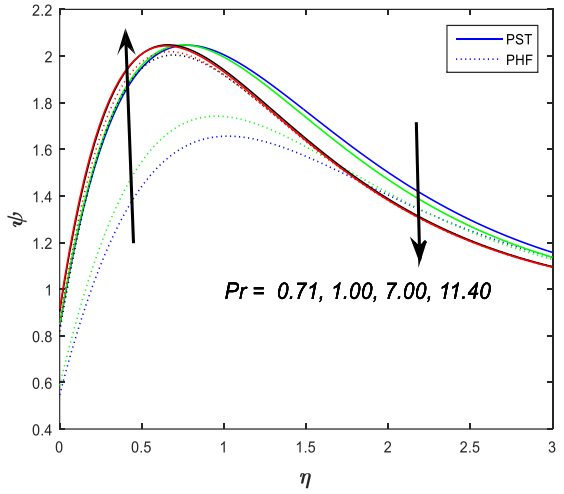


Fig. 15: Influence of Pr on velocity profiles

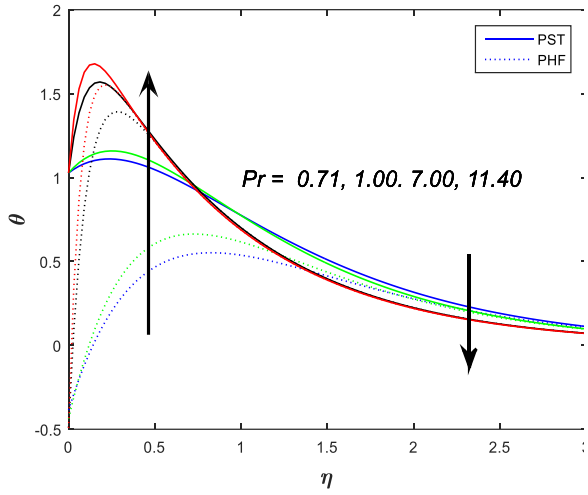


Fig. 16: Influence of Pr on temperature profiles

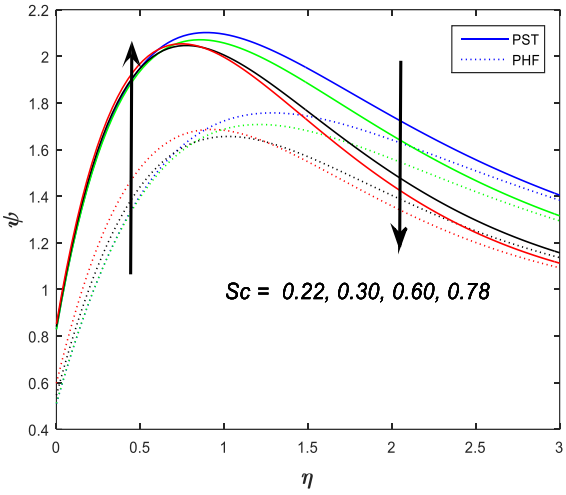


Fig. 17: Influence of *Sc* on velocity profiles

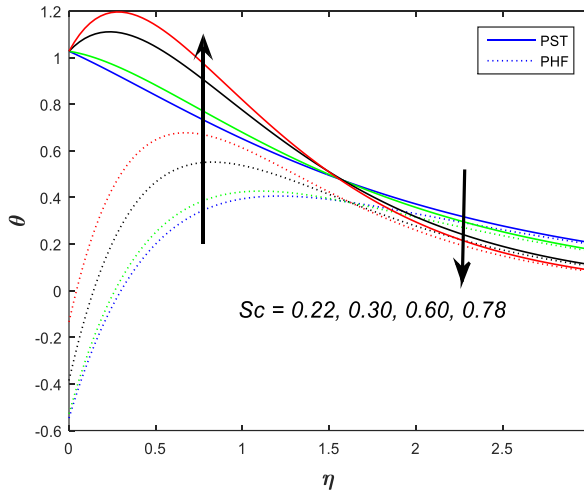


Fig. 18: Influence of *Sc* on temperature profiles

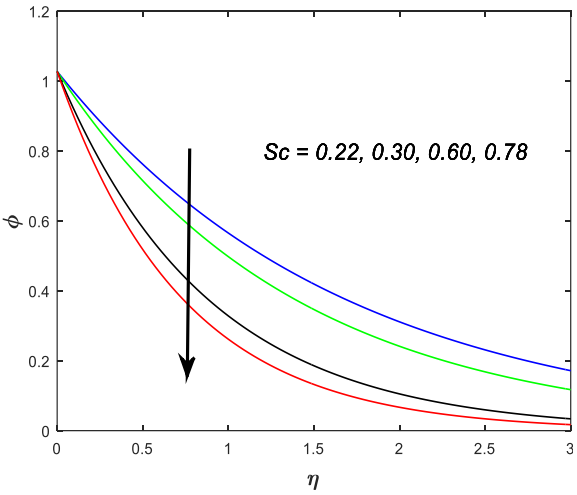


Fig. 19: Influence of *Sc* on concentration profiles

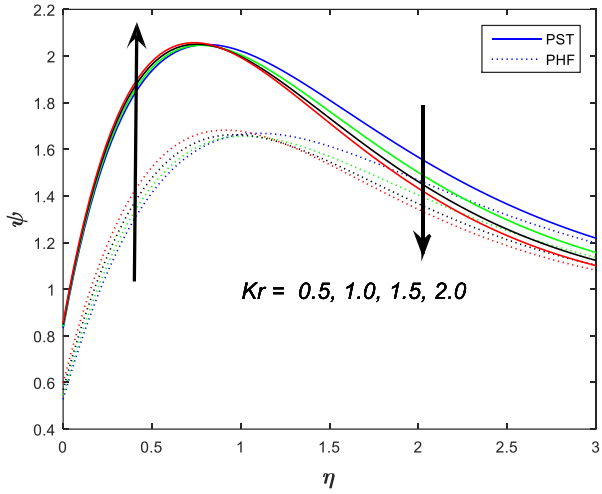


Fig. 20: Influence of $Kr$ on velocity profiles

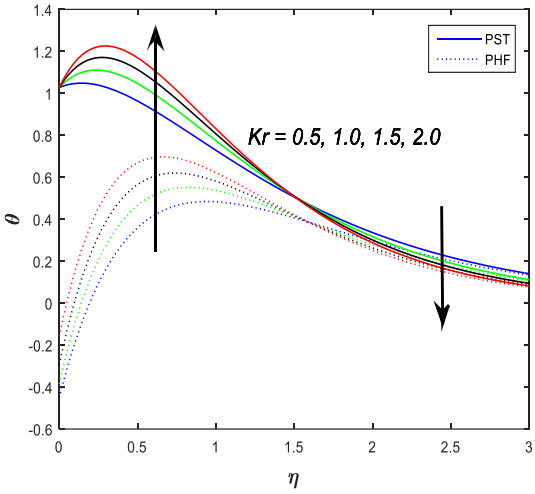


Fig. 21: Influence of $Kr$ on temperature profiles

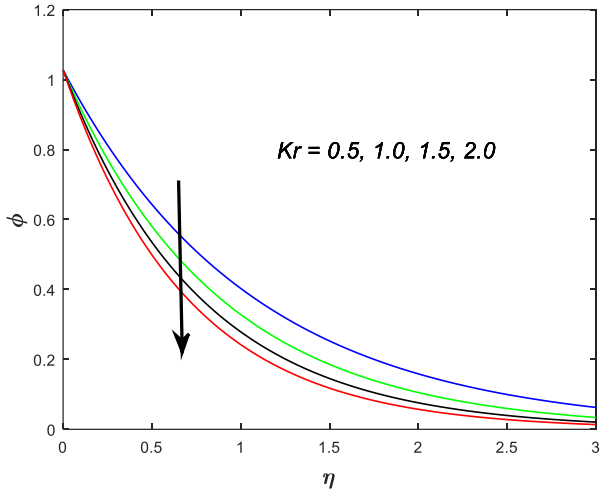


Fig. 22: Influence of $Kr$ on concentration profiles

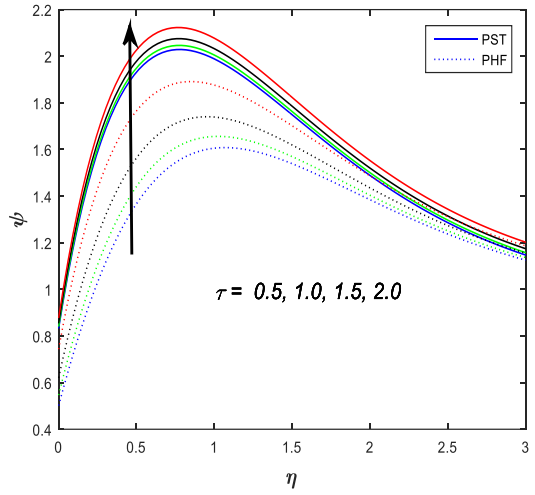


Fig. 23: Influence of $\tau$ on velocity profiles

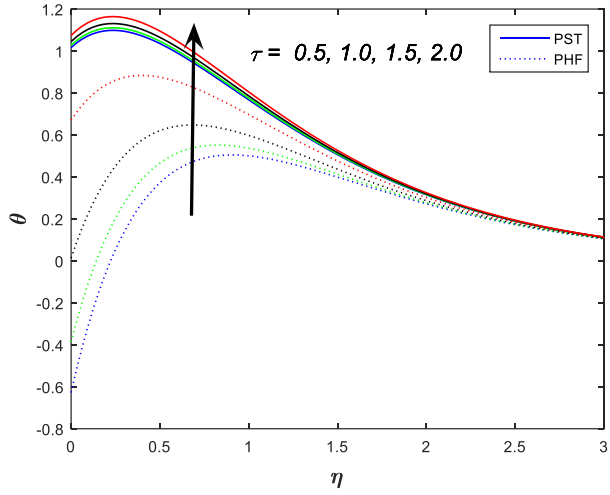


Fig. 24: Influence of $\tau$ on temperature profiles

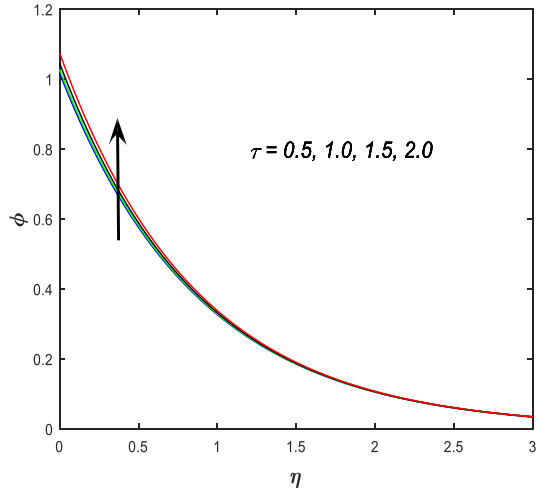


Fig. 25: Influence of $\tau$ on concentration profiles

Fig. 6 shows the fluid velocity profile variations with the slip parameter. It is observed that, the fluid velocity increases on increasing the slip parameter, thus enhancing the fluid flow for both PST and PHF boundary conditions. It is observed that from Figs.7 and 8, both the fluid velocity and temperature decreases on increasing the radiation parameter for both PST and PHF boundary conditions. Figs. 9 and 10 demonstrate the plot of fluid velocity and temperature for a variety of heat source parameter. It is seen in figures that, the fluid velocity and temperature decrease on increasing the heat source parameter. This implies that heat source tend to retard the fluid velocity and temperature for both PST and PHF boundary conditions. This is because radiation and heat absorption have tendency to reduce fluid temperature. Figs. 11 and 12 depict effect of radiation of absorption parameter on the fluid velocity and temperature in both cases PST and PHF. The velocity and temperature are found to increases on increasing radiation of absorption parameter.

The influence of Dufour number on velocity and temperature profiles are plotted in Figs. 13 and 14 respectively. The Dufour number signifies the contribution of the concentration gradient to the thermal energy flux in the flow. It is found that an increase in the Dufour number causes an enhancement in velocity and temperature under the PST and PHF boundary conditions. Figs. 15 and 16 show the plot of velocity and temperature of the flow field against different values of Prandtl number taking other parameters are constant in both cases PST and PHF. The Prandtl number defines the ratio of momentum diffusivity to thermal diffusivity. The Prandtl number values are chosen for air $(\mathrm{Pr} = 0.71)$, electrolytic solution $(\mathrm{Pr} = 1.00)$, water $(\mathrm{Pr} = 7.00)$ and water at $4^0C$ $(\mathrm{Pr} = 11.40)$. It is evident from Figs. 15 and 16, velocity and temperature profiles are increases in a region near to the plate and decreases in a region away from the plate for both PST and PHF boundary conditions on increasing the Prandtl number. Thus higher Prandtl number leads to faster cooling of the plate.

The nature of the fluid velocity, temperature and concentration in the presence of foreign species such as Hydrogen $(Sc = 0.22)$, Helium $(Sc = 0.30)$, Water vapour $(Sc = 0.60)$, Ammonia $(Sc = 0.78)$ is shown in Figs. 17 to 19. Physically, Schmidt number signifies the relative strength of viscosity to chemical molecular diffusivity. It is observed that, velocity and temperature increases on increasing the Schmidt number in a region near to the plate whereas they are decreases in a region away from the plate for both PST and PHF boundary conditions. The flow field decelerate the velocity and temperature in the presence of heavier diffusing species. Schmidt number is found to decrease the concentration of the flow field at all points.

Table 2: Influence of $Gr, Gm, M, K$, and $Du$ on the skin friction coefficient.

| $Gr$ | $Gm$ | $M$ | $K$ | $Du$ | Skin friction coefficient $C_f$ | |
|---|---|---|---|---|---|---|
| | | | | | PST | PHF |
| 1.0 | 2.0 | 2.0 | 5.0 | 5.0 | 2.5736 | 2.2059 |
| 2.0 | 2.0 | 2.0 | 5.0 | 5.0 | 3.1165 | 2.3812 |
| 3.0 | 2.0 | 2.0 | 5.0 | 5.0 | 3.6595 | 2.5565 |
| 4.0 | 2.0 | 2.0 | 5.0 | 5.0 | 4.2025 | 2.7318 |
| 4.0 | 0.5 | 2.0 | 5.0 | 5.0 | 3.7094 | 2.2386 |
| 4.0 | 1.0 | 2.0 | 5.0 | 5.0 | 3.8738 | 2.4030 |
| 4.0 | 1.5 | 2.0 | 5.0 | 5.0 | 4.0381 | 2.5674 |
| 4.0 | 2.0 | 2.0 | 5.0 | 5.0 | 4.2025 | 2.7318 |
| 4.0 | 2.0 | 1.0 | 5.0 | 5.0 | 4.8124 | 3.0141 |
| 4.0 | 2.0 | 2.0 | 5.0 | 5.0 | 4.2025 | 2.7318 |
| 4.0 | 2.0 | 3.0 | 5.0 | 5.0 | 3.8845 | 2.6133 |
| 4.0 | 2.0 | 4.0 | 5.0 | 5.0 | 3.6926 | 2.5608 |
| 4.0 | 2.0 | 2.0 | 0.5 | 5.0 | 2.9432 | 1.7868 |
| 4.0 | 2.0 | 2.0 | 1.0 | 5.0 | 3.5044 | 2.1994 |
| 4.0 | 2.0 | 2.0 | 1.5 | 5.0 | 3.7576 | 2.3902 |
| 4.0 | 2.0 | 2.0 | 2.0 | 5.0 | 3.9024 | 2.5005 |
| 4.0 | 2.0 | 2.0 | 5.0 | 0.5 | 3.3892 | 1.7951 |
| 4.0 | 2.0 | 2.0 | 5.0 | 1.0 | 3.4796 | 1.8992 |
| 4.0 | 2.0 | 2.0 | 5.0 | 1.5 | 3.5700 | 2.0033 |
| 4.0 | 2.0 | 2.0 | 5.0 | 2.0 | 3.6603 | 2.1073 |

Table 3: Influence of $Pr, N, H$ and $Q$ on the skin friction coefficient.

| $Pr$ | $N$ | $H$ | $Q$ | Skin friction coefficient $C_f$ | |
|---|---|---|---|---|---|
| | | | | PST | PHF |
| 0.71 | 2.0 | 1.0 | 2.0 | 4.2025 | 2.7318 |
| 1.00 | 2.0 | 1.0 | 2.0 | 4.2414 | 2.9346 |
| 7.00 | 2.0 | 1.0 | 2.0 | 4.5203 | 4.0930 |
| 11.40 | 2.0 | 1.0 | 2.0 | 4.5756 | 4.2817 |
| 0.71 | 0.5 | 1.0 | 2.0 | 4.8553 | 3.3838 |
| 0.71 | 1.0 | 1.0 | 2.0 | 4.5770 | 3.0642 |
| 0.71 | 1.5 | 1.0 | 2.0 | 4.3677 | 2.8681 |
| 0.71 | 2.0 | 1.0 | 2.0 | 4.2025 | 2.7318 |
| 0.71 | 2.0 | 0.2 | 2.0 | 4.4867 | 2.9760 |
| 0.71 | 2.0 | 0.4 | 2.0 | 4.4054 | 2.9013 |
| 0.71 | 2.0 | 0.6 | 2.0 | 4.3317 | 2.8371 |
| 0.71 | 2.0 | 0.8 | 2.0 | 4.2643 | 2.7811 |
| 0.71 | 2.0 | 1.0 | 0.5 | 3.9933 | 2.5026 |
| 0.71 | 2.0 | 1.0 | 1.0 | 4.0630 | 2.5790 |
| 0.71 | 2.0 | 1.0 | 1.5 | 4.1327 | 2.6554 |
| 0.71 | 2.0 | 1.0 | 2.0 | 4.2025 | 2.7318 |

Table 4: Influence of $Sc, Kr, h$ and $\tau$ on the skin friction coefficient.

| $Sc$ | $Kr$ | $h$ | $\tau$ | Skin friction coefficient $C_f$ | |
|---|---|---|---|---|---|
| | | | | PST | PHF |
| 0.22 | 1.0 | 0.2 | 1.0 | 4.1502 | 2.5518 |
| 0.30 | 1.0 | 0.2 | 1.0 | 4.1517 | 2.5927 |
| 0.60 | 1.0 | 0.2 | 1.0 | 4.2025 | 2.7318 |
| 0.78 | 1.0 | 0.2 | 1.0 | 4.2605 | 2.9886 |
| 0.60 | 0.5 | 0.2 | 1.0 | 4.1614 | 2.6383 |
| 0.60 | 1.0 | 0.2 | 1.0 | 4.2025 | 2.7318 |
| 0.60 | 1.5 | 0.2 | 1.0 | 4.2435 | 2.8452 |
| 0.60 | 2.0 | 0.2 | 1.0 | 4.2815 | 2.9906 |
| 0.60 | 1.0 | 0.1 | 1.0 | 4.9262 | 3.2118 |
| 0.60 | 1.0 | 0.2 | 1.0 | 4.2025 | 2.7318 |
| 0.60 | 1.0 | 0.3 | 1.0 | 3.6643 | 2.3767 |
| 0.60 | 1.0 | 0.4 | 1.0 | 3.2483 | 2.1034 |
| 0.60 | 1.0 | 0.2 | 0.5 | 4.1606 | 2.5062 |
| 0.60 | 1.0 | 0.2 | 1.0 | 4.2025 | 2.7318 |
| 0.60 | 1.0 | 0.2 | 1.5 | 4.2716 | 3.1036 |
| 0.60 | 1.0 | 0.2 | 2.0 | 4.3856 | 3.7167 |

It is observed that from Figs. 20 and 22, the fluid velocity and temperature profiles are increases on increasing the chemical reaction parameter in a region near to the plate but them decreases in the region away from the plate for both PST and PHF boundary conditions. Species concentration decreases on increasing the chemical reaction parameter. This implies that the chemical reaction parameter retard the fluid velocity, temperature and concentration. It is also noted from Figs. 23 to 25 that the fluid velocity, temperature and concentration profiles are increases with the progress of time for both PST and PHF boundary conditions.

It is evident from Tables 2 to 4 that the skin friction coefficient at the plate declines on increasing the Magnetic parameter, radiation parameter, heat source parameter, and slip parameter whereas it accelerates upon increasing the thermal Grashof number, solutal Grashof number, permeability parameter, Dufour number, Prandtl number, radiation of absorption parameter, Schmidt number, and chemical reaction parameter for both PST and PHF boundary conditions. Shear stress at the plate is getting enhanced with the progress of time for both PST and PHF boundary conditions.

Table 5: Influence of $Pr, N, H$ and $Q$ on the heat transfer coefficient.

| $Pr$ | $N$ | $H$ | $Q$ | Heat transfer coefficient $Nu$ | |
|---|---|---|---|---|---|
| | | | | PST | PHF |
| 0.71 | 2.0 | 1.0 | 2.0 | -0.7972 | -3.3023 |
| 1.00 | 2.0 | 1.0 | 2.0 | -1.2020 | -4.4513 |
| 7.00 | 2.0 | 1.0 | 2.0 | -8.4131 | -22.3422 |
| 11.40 | 2.0 | 1.0 | 2.0 | -13.3477 | -34.3524 |
| 0.71 | 0.5 | 1.0 | 2.0 | -1.8069 | -3.1715 |
| 0.71 | 1.0 | 1.0 | 2.0 | -1.4055 | -3.2722 |
| 0.71 | 1.5 | 1.0 | 2.0 | -1.0770 | -3.2978 |
| 0.71 | 2.0 | 1.0 | 2.0 | -0.7972 | -3.3023 |
| 0.71 | 2.0 | 0.2 | 2.0 | -1.2670 | -3.2869 |
| 0.71 | 2.0 | 0.4 | 2.0 | -1.1382 | -3.2952 |
| 0.71 | 2.0 | 0.6 | 2.0 | -1.0176 | -3.2996 |
| 0.71 | 2.0 | 0.8 | 2.0 | -0.9043 | -3.3017 |
| 0.71 | 2.0 | 1.0 | 0.5 | -0.3193 | -2.8767 |
| 0.71 | 2.0 | 1.0 | 1.0 | -0.4786 | -3.0185 |
| 0.71 | 2.0 | 1.0 | 1.5 | -0.6379 | -3.1604 |
| 0.71 | 2.0 | 1.0 | 2.0 | -0.7972 | -3.3023 |

Table 6: Influence of $Du, Sc, Kr$ and $\tau$ on the heat transfer coefficient.

| $Du$ | $Sc$ | $Kr$ | $\tau$ | Heat transfer coefficient $Nu$ | |
|---|---|---|---|---|---|
| | | | | PST | PHF |
| 0.5 | 0.60 | 1.0 | 1.0 | -1.0738 | -1.7550 |
| 1.0 | 0.60 | 1.0 | 1.0 | -0.8660 | -1.9269 |
| 1.5 | 0.60 | 1.0 | 1.0 | -0.6581 | -2.0988 |
| 2.0 | 0.60 | 1.0 | 1.0 | -0.4502 | -2.2708 |
| 5.0 | 0.22 | 1.0 | 1.0 | -0.3362 | -2.5039 |
| 5.0 | 0.30 | 1.0 | 1.0 | -0.4828 | -3.1266 |
| 5.0 | 0.60 | 1.0 | 1.0 | -0.7972 | -3.3023 |
| 5.0 | 0.78 | 1.0 | 1.0 | -1.3792 | -3.3625 |
| 5.0 | 0.60 | 0.5 | 1.0 | -0.3207 | -2.9630 |
| 5.0 | 0.60 | 1.0 | 1.0 | -0.7972 | -3.3023 |
| 5.0 | 0.60 | 1.5 | 1.0 | -1.2103 | -3.5252 |
| 5.0 | 0.60 | 2.0 | 1.0 | -1.5830 | -3.6161 |
| 5.0 | 0.60 | 1.0 | 0.5 | -0.7822 | -3.7629 |
| 5.0 | 0.60 | 1.0 | 1.0 | -0.7972 | -3.3023 |
| 5.0 | 0.60 | 1.0 | 1.5 | -0.8220 | -2.5428 |
| 5.0 | 0.60 | 1.0 | 2.0 | -0.8629 | -1.2907 |

Table 7: Influence of $Sc, Kr$ and $\tau$ on the mass transfer coefficient.

| $Sc$ | $Kr$ | $\tau$ | Mass transfer coefficient $Sh$ |
|---|---|---|---|
| 0.22 | 1.0 | 1.0 | -0.6146 |
| 0.30 | 1.0 | 1.0 | -0.7456 |
| 0.60 | 1.0 | 1.0 | -1.1744 |
| 0.78 | 1.0 | 1.0 | -1.4079 |
| 0.60 | 0.5 | 1.0 | -0.9644 |
| 0.60 | 1.0 | 1.0 | -1.1744 |
| 0.60 | 1.5 | 1.0 | -1.3421 |
| 0.60 | 2.0 | 1.0 | -1.4860 |
| 0.60 | 1.0 | 0.5 | -1.1572 |
| 0.60 | 2.0 | 1.0 | -1.1744 |
| 0.60 | 3.0 | 1.5 | -1.2027 |
| 0.60 | 4.0 | 2.0 | -1.2495 |

It is clear from Tables 5 and 6 that heat transfer coefficient decreases on increasing the Prandtl number, radiation of absorption parameter, Schmidt number, and chemical reaction parameter for both PST and PHF boundary conditions. Also the rate of heat transfer at the plate increases for PST but decreases for PHF on increasing the radiation parameter, heat source parameter and Dufour number. Rate of heat transfer at the plate is getting enhanced for PHF whereas it is getting reduced for PST with the progress of time.

## 6. Conclusions

From the present investigation, following conclusions can be drawn:

- Velocity profiles are increases in a region near to the plate and decreases in a region away from the plate on increasing the Prandtl number, Schmidt number, and chemical reaction parameter whereas the skin friction coefficient increases for both PST and PHF boundary conditions.
- Slip parameter accelerate the fluid velocity whereas it has a reverse effect on skin friction coefficient for both PST and PHF boundary conditions.
- Radiation parameter and heat source parameter are tending to retard the fluid temperature whereas radiation of absorption parameter, Dufour number and time has a reverse on it for both PST and PHF boundary conditions.
- Heat transfer coefficient increases for PST and decreases for PHF on increasing the Dufour number, radiation parameter and heat source parameter but it decreases for PST and increases for PHF with progress of time.
- Concentration increases whereas mass transfer coefficient decreases with the progress of time.

## Acknowledgements

It is pleasure to declare our transparent appreciation to the reviewers for their constructive suggestions and comments for renovation of this article.

## References

Adesanya, S. O. and Makinde, O. D. (2014): MHD oscillatory slip flow and heat transfer in a channel filled with porous media, U.P.B. Sci. Bull., Series A, Vol. 76, No. 1, pp.197-204.

Baitharu, A. P., Sahoo, S. and Dash, G. C. (2020): Heat and mass transfer effect on a radiative second grade MHD flow in a porous medium over a stretching sheet, Journal of Naval Architecture and Marine Engineering, Vol. 17, No. 1, pp. 51-66. https://doi.org/10.3329/jname.v17i1.37777

Balamurugan, K. S., Rajakumar, K. V. B. and Rama Prasad, J. L. (2021): Cosinusoidally fluctuating temperature and chemical reacting effects on MHD-free convective fluid flow past a vertical porous plate with Hall, Ion-slip current, and Soret, Lecture Notes in Mechanical Engineering. Springer, Singapore, pp. 15-24. https://doi.org/10.1007/978-981-15-4308-1_2

Cramer, K. R. and Pai S. I. (1973): Magnetofluid dynamics for engineers and applied physicists, McGraw Hill Book Company, New York.

Kim, Y. J. (2000): Unsteady MHD convective heat transfer past a semi-infinite vertical porous moving plate with variable suction, International Journal of Engineering Science, Vol. 38, No. 8, pp. 833-845. https://doi.org/10.1016/S0020-7225(99)00063-4

Makinde, O. D. (2011): On MHD mixed convection with Soret and Dufour effects past a vertical plate embedded in a porous medium, Latin American Applied Research, Vol. 41, No. 1, pp. 63-68.

Malapati, V. and Dasari, V. L. (2017): Soret and chemical reaction effects on the radiative MHD flow from an infinite vertical plate, J. Korean Soc. Ind. Appl. Math, Vol. 21, No. 1, pp. 39-61. https://doi.org/10.12941/jksiam.2017.21.039

Manjula, J., Padma, P., Gnaneswara Reddy, M. and Venakateswarlu, M. (2015): Influence of thermal radiation and chemical reaction on MHD flow, heat and mass transfer over a stretching surface, Procedia Engineering, Vol.127, pp. 1315-1322. https://doi.org/10.1016/j.proeng.2015.11.489

Nield, D. A., and Bejan A. (1999): Convection in Porous Media, 2nd edition, Springer Verlag, New York, 1999.

Pal, D. and Talukdar, B. (2010): Perturbation analysis of unsteady magnetohydrodynamic convective heat and mass transfer in a boundary layer slip flow past a vertical permeable plate with thermal radiation and chemical reaction, Commun Nonlinear Sci Numer Simulat, Vol. 15, No. 7, pp. 1813-1830.

https://doi.org/10.1016/j.cnsns.2009.07.011
Rajakumar, K. V. B., Balamurugan, K. S. and Ramana Murthy, Ch. V. (2018a): Radiation absorption and viscous-dissipation effects on magnetohydrodynamic free-convective flow past a semi-infinite, moving, vertical, porous plate, International Journal of Fluid Mechanics Research, Vol. 45, No. 5, pp. 439-458. https://dx.doi.org/10.1615/InterJFluidMechRes.2018024790
Rajakumar, K. V. B., Balamurugan, K. S., Umasankara Reddy, M. and Ramana Murthy, Ch. V. (2018b): Radiation, dissipation and Dufour effects on MHD free convection Casson fluid flow through a vertical oscillatory porous plate with ion-slip current, International Journal of Heat and Technology, Vol. 36, No. 2, pp. 494-508. https://doi.org/ 10.18280/ijht.360214
Rajakumar, K. V. B., Govinda Rao, T., Umasankara Reddy, M. and Balamurugan, K. S. (2020a): Influence of Dufour and thermal radiation on unsteady MHD Walter's liquid model-B flow past an impulsively started infinite vertical plate embedded in a porous medium with chemical reaction, Hall and ion slip current, SN Appl. Sci. vol. 2, Article ID: 742. https://doi.org/10.1007/s42452-020-2484-y
Rajakumar, K. V. B., Rayaprolu, V. S. R. P. K., Balamurugan, K. S. and Kumar, V. B. (2020b): Unsteady MHD Casson dissipative fluid flow past a semi-infinite vertical porous plate with radiation absorption and chemical reaction in presence of heat generation, Mathematical Modelling of Engineering Problems, Vol. 7, No. 1, pp. 160-172. https://doi.org/10.18280/mmep.070120
Rajput, U. S. and Kumar, G. (2019): Effects of radiation and chemical reaction on MHD flow past a vertical plate with variable temperature and mass diffusion, Journal of Naval Architecture and Marine Engineering, Vol. 16, No. 2, pp. 99-108. https://doi.org/10.3329/jname.v16i2.29526
Raju, M. C., Harinath Reddy, S. and Keshava Reddy, E. (2018): Study of ramped temperature influence on MHD convective chemically reactive and absorbing fluid past an exponentially accelerated vertical porous plate, Journal of Naval Architecture and Marine Engineering, Vol. 15, No. 2, pp. 107-125. https://doi.org/10.3329/jname.v15i2.31314
Raptis, A. (2011): Free convective oscillatory flow and mass transfer past a porous plate in the presence of radiation for an optically thin fluid, Thermal Sci, Vol.15, No.3, pp. 849-857. https://doi.org/10.2298/tsci101208032r
Rout, B., Mishra, S. and Tirupati, T. (2019): Effect of viscous dissipation on Cu-water and Cu-kerosene nanofluids of axisymmetric radiative squeezing flow, Heat Transfer Asian Research, Vol. 48, No. 7, pp. 3039-3054. https://doi.org/10.1002/htj.21529
Rout, P. K., Sahoo, S. N. and Dash, G. C. (2016): Effect of heat source and chemical reaction on MHD flow past a vertical plate with variable temperature, Journal of Naval Architecture and Marine Engineering, Vol. 13, No. 1, pp. 101-110. https://doi.org/10.3329/jname.v13i1.23930
Seini, Y. I. and Makinde, O. D. (2013): Hydromagnetic flow with Dufour and Soret effects past a vertical plate embedded in porous media, Mathematical Theory and Modeling, Vol.3, No.12, pp.47-64.
Seth, G. S., Tripathi, R., Sharma, R. and Chamkha, A. J. (2017): MHD double diffusive natural convection flow over exponentially accelerated inclined plate, Journal of Mechanics, Vol. 33, No.1, pp. 87-99. https://doi.org/10.1017/.2016.56
Shankar Goud, B., Dharmendar Reddy, Y. and Srinivasa Rao, V. (2020): Thermal radiation and Joule heating effects on a magnetohydrodynamic Casson nanofluid flow in the presence of chemical reaction through a non-linear inclined porous stretching sheet, Journal of Naval Architecture and Marine Engineering, Vol. 17, No. 2, pp. 143-164. https://doi.org/10.3329/jname.v17i2.49978
Sharma, P. and Saboo, R. (2017): Heat and mass transfer with viscous dissipation in horizontal channel partially occupied by porous medium in the presence of oscillatory suction, Journal of Naval Architecture and Marine Engineering, vol. 14, no. 2, pp. 101-114. https://doi.org/10.3329/jname.v14i2.25584
Siva Kumar, N., Rushi Kumar. and A. G. Vijaya Kumar, A. G. (2016): Thermal diffusion and chemical reaction effects on unsteady flow past a vertical porous plate with heat source dependent in slip flow regime, Journal of Naval Architecture and Marine Engineering, Vol. 13, No. 1, pp. 51-62. https://doi.org/10.3329/jname.v13i1.20773
Sparrow, E. M. and Cess, R. D. (1961): Temperature dependent heat sources or sinks in a stagnation point flow, Appl. Sci. Res., Vol. 10, pp. 185-197.
Thirupathi, T. and Mishra, S. R. (2018): Effect of viscous dissipation and Joule heating on magnetohydrodynamic Jeffery nanofluid flow with and without multi slip boundary conditions, Journal of Nanofluids, Vol. 7, No. 3, pp. 516-526. https://doi.org/10.1166/jon.2018.1469
Thirupathi, T. and Satya Narayana, P. V. (2020): Innovations in Eyring-Powell radiative nanofluid flow due to nonlinear stretching sheet with convective heat and mass conditions: Numerical study, Australian Journal of Mechanical Engineering, https://doi.org/10.1080/14484846.2020.1842158

Tirupathi, T. and Magagula, V. M. (2020): Transient electromagnetohydrodynamic radiative squeezing flow between two parallel Riga plates using a spectral local linearization approach, Heat Transfer Asian Research, Vol. 49, No. 1, pp. 67-85. https://doi.org/10.1002/htj.21599

Tirupati, T., Wakif, A. and Animasaun, I. L. (2020): Generalized differential quadrature analysis of unsteady three-dimensional MHD radiating dissipative Casson fluid conveying tiny particles, Heat Transfer Asian Research, Vol. 49, No. 5, pp. 2595-2626. https://doi.org/10.1002/htj.21736

Vedavathi, N., Ramakrishna, K. and Reddy, K. J. (2015): Radiation and mass transfer effects on unsteady MHD convective flow past an infinite vertical plate with Dufour and Soret effects, Ain Shams Engineering Journal, vol. 6, pp. 363-371. https://doi.org/10.1016/j.asej.2014.09.009

Venkateswarlu, M. and Padma, P. (2015): Unsteady MHD free convective heat and mass transfer in a boundary layer flow past a vertical permeable plate with thermal radiation and chemical reaction, Procedia Engineering, Vol.127, pp. 791-799. https://doi.org/10.1016/j.proeng.2015.11.414

Venkateswarlu, M. and Bhaskar, P. (2020): Entropy generation and Bejan number analysis of MHD Casson fluid flow in a micro-channel with Navier slip and convective boundary conditions, International Journal of Thermofluid Science and Technology, Vol. 7, No. 4, pp. 1-22. Paper No: 070403. https://doi.org/10.36963/IJTST.2020070403

Venkateswarlu, M. and Makinde, O. D. (2018): Unsteady MHD slip flow with radiative heat and mass transfer over an inclined plate embedded in a porous medium, Defect and Diffusion Forum, vol. 384, pp. 31-48. https://doi.org/10.4028/www.scientific.net/DDF.384.31

Venkateswarlu, M. and Phani kumar, M. (2017): Soret and heat source effects on MHD flow of a viscous fluid in a parallel porous plate channel in presence of slip condition, U. P. B. Sci. Bull., Series D: Mechanical Engineering, Vol. 79, No. 4, pp. 171- 186.

Venkateswarlu, M. and Venkata Lakshmi, D. (2016): Slip velocity distribution on MHD oscillatory heat and mass transfer flow of a viscous fluid in a parallel plate channel, GANIT J. Bangladesh Math. Soc, Vol.36, pp. 91-112. https://doi.org/10.3329/ganit.v36i0.32776

Venkateswarlu, M. and Venkata Lakshmi, D. (2017): Thermal diffusion, hall current and chemical reaction effects on unsteady MHD natural convective flow past a vertical plate, U. P. B. Sci. Bull., Series D: Mechanical Engineering., Vol. 79, No. 1, pp. 91-106.

Venkateswarlu, M., Venkata Lakshmi, D. and Darmaiah, G. (2016): Influence of slip condition on radiative MHD flow of a viscous fluid in a parallel porous plate channel in presence of heat absorption and chemical reaction , J. Korean Soc. Ind. Appl. Math., Vol. 20, No. 4, pp. 333-354. https://doi.org/10.12941/jksiam.2016.20.333

Venkateswarlu, M., Bhaskar, P. and Venkata Lakshmi, D. (2019a): Soret and Dufour effects on radiative hydromagnetic flow of a chemically reacting fluid over an exponentially accelerated inclined porous plate in presence of heat absorption and viscous dissipation, J. Korean Soc. Ind. Appl. Math, Vol. 23, No. 3, pp. 157-178. https://doi.org/10.12941/jksiam.2019.23.157

Venkateswarlu, M., Makinde, O. D. and Lakshmi, D. V. (2019b): Influence of thermal radiation and heat generation on steady hydromagnetic flow in a vertical micro-porous-channel in presence of suction/injection, Journal of Nanofluids, Vol. 8, No. 5, pp. 1010-1019. https://doi.org/10.1166/jon.2019.1647

Venkateswarlu, M., Makinde, O. D. and Rami Reddy, P. (2019c): Influence of Hall current and thermal diffusion on radiative hydromagnetic flow of a rotating fluid in presence of heat absorption, Journal of Nanofluids, Vol. 8, No. 4, pp. 756-766. https://doi.org/10.1166/jon.2019.1638

Venkateswarlu, M., Prameela, M. and Makinde, O. D. (2019d): Influence of heat generation and viscous dissipation on hydromagnetic fully developed natural convection flow in a vertical micro–channel, Journal of Nanofluids, Vol. 8, No. 7, pp. 1506-1516. https://doi.org/10.1166/jon.2019.1692

Venkateswarlu, M., Upender Reddy, G. and Venkata Lakshmi, D. (2018): Influence of Hall current and heat source on MHD flow of a rotating fluid in a parallel porous plate channel, J. Korean Soc. Ind. Appl. Math, Vol. 22, No. 4, pp. 217-239. https://doi.org/10.12941/jksiam.2018.22.217

Venkateswarlu, M., Venkata Lakshmi, D. and Makinde, O. D. (2020): Thermodynamics analysis of Hall current and Soret number on hydromagnetic couette flow in a rotating system with a convective boundary condition, Heat Transfer Research, Vol. 51, No. 1, pp. 83-101. https://doi.org/10.1615/HeatTransRes.2019027139

## Appendix

$$m_1=\frac{Sc+\sqrt{Sc^2+4ScKr}}{2},\ m_2=\frac{Sc+\sqrt{Sc^2+4Sc\left(Kr+\omega\right)}}{2},\ m_3=\frac{\Pr+\sqrt{\Pr^2+4\Pr\left(N+H\right)}}{2},$$

$$m_4=\frac{\Pr+\sqrt{\Pr^2+4\Pr\left(N+H+\omega\right)}}{2},\ m_5=\frac{1+\sqrt{1+4\left(M+\frac{1}{K}\right)}}{2},\ m_6=\frac{1+\sqrt{1+4\left(M+\frac{1}{K}+\omega\right)}}{2},$$

$$A_1=AScm_1,\ A_2=m_1^2-Scm_1-Sc\left(Kr+\omega\right),\ A_3=\frac{A_1}{A_2},\ A_4=1-A_3,\ A_5=\Pr\left[Dum_1^2+Q\right],$$

$$A_6=m_1^2-\Pr m_1-\Pr\left(N+H\right),\ A_7=\frac{A_5}{A_6},\ A_8=1+A_7,\ A_9=\Pr\left[DuA_3m_1^2+QA_3+Am_1A_7\right],$$

$$A_{10}=\Pr A_4\left[Dum_2^2+Q\right],\ A_{11}=A\Pr m_3A_8,\ A_{12}=m_1^2-\Pr m_1-\Pr\left(N+H+\omega\right),$$

$$A_{13}=m_2^2-\Pr m_2-\Pr\left(N+H+\omega\right),\ A_{14}=m_3^2-\Pr m_3-\Pr\left(N+H+\omega\right),\ A_{15}=\frac{A_9}{A_{12}},\ A_{16}=\frac{A_{10}}{A_{13}},$$

$$A_{17}=\frac{A_{11}}{A_{14}},\ A_{18}=1+A_{15}+A_{16}-A_{17},\ A_{19}=m_1^2-m_1-\left(M+\frac{1}{K}\right),\ A_{20}=m_3^2-m_3-\left(M+\frac{1}{K}\right),$$

$$A_{21}=\frac{GrA_7-Gm}{A_{19}},\ A_{22}=\frac{GrA_8}{A_{20}},\ A_{23}=1+hm_1,\ A_{24}=1+hm_3,\ A_{25}=1+hm_5,\ A_{26}=A_{22}A_{24}-\left(A_{21}A_{23}+1\right)$$

$$,\ A_{27}=\frac{A_{26}}{A_{25}},\ A_{28}=GrA_{15}-GmA_3+Am_1A_{21},\ A_{29}=GrA_{16}-GmA_4,\ A_{30}=GrA_{17}+Am_3A_{22},\ A_{31}=GrA_{18},$$

$$A_{32}=Am_5A_{27},\ A_{33}=m_1^2-m_1-\left(M+\frac{1}{K}+\omega\right),\ A_{34}=m_2^2-m_2-\left(M+\frac{1}{K}+\omega\right),$$

$$A_{35}=m_3^2-m_3-\left(M+\frac{1}{K}+\omega\right),\ A_{36}=m_4^2-m_4-\left(M+\frac{1}{K}+\omega\right),\ A_{37}=m_5^2-m_5-\left(M+\frac{1}{K}+\omega\right),$$

$$A_{38}=\frac{A_{28}}{A_{33}},\ A_{39}=\frac{A_{29}}{A_{34}},\ A_{40}=\frac{A_{30}}{A_{35}},\ A_{41}=\frac{A_{31}}{A_{36}},\ A_{42}=\frac{A_{32}}{A_{37}},\ A_{43}=1+hm_2,\ A_{44}=1+hm_4,\ A_{45}=1+hm_6,$$

$$A_{46}=A_{40}A_{24}+A_{41}A_{44}-\left(A_{38}A_{23}+A_{39}A_{43}+A_{25}A_{23}+1\right),\ A_{47}=\frac{A_{46}}{A_{45}},\ B_1=A_7-1,\ B_2=A\Pr m_3B_1,$$

$$B_3=\frac{B_2}{A_{14}},\ B_4=\left(A_{15}+A_{16}\right)-\left(1+B_3\right),\ B_5=\frac{GrB_1}{A_{20}},\ B_6=B_5A_{24}-\left(A_{21}A_{23}+1\right),\ B_7=\frac{B_6}{A_{25}},$$

$$B_8=GrB_3+Am_3B_5,\ B_9=GrB_4,\ B_{10}=Am_5B_7,\ B_{11}=\frac{B_8}{A_{35}},\ B_{12}=\frac{B_9}{A_{36}},\ B_{13}=\frac{B_{10}}{A_{37}},$$

$$B_{14}=B_{11}A_{24}+B_{12}A_{44}-\left(A_{38}A_{23}+A_{39}A_{42}+B_{13}A_{25}+1\right),\ B_{15}=\frac{B_{14}}{A_{45}}.$$